Catal Lett (2008) 124:34–38
DOI 10.1007/s10562-008-9503-8

Graphite Oxide as a Novel Host Material of Catalytically Active Pd Nanoparticles

Ágnes Mastalir · Zoltán Király · Mária Benkő · Imre Dékány

Received: 17 March 2008 / Accepted: 23 April 2008 / Published online: 17 May 2008

Abstract Graphite oxide (GO) was utilized as a novel host material for Pd nanoparticles of controlled crystallite size. Immobilization of the Pd nanoparticles from a stable Pd sol in GO resulted in the formation of organophilic Pd–GO, a layer-structured material, which was characterized by ICP-AES, XRD and TEM. Pd–GO proved to be a highly active and stereoselective catalyst in liquid-phase alkyne hydrogenations under mild conditions.

Keywords Graphite oxide · Palladium · Nanoparticle · X-ray diffraction · Transmission electron microscopy · Alkyne hydrogenation · Turnover frequency · Selectivity

1 Introduction

Graphite oxide (GO) is an oxygen-rich carbonaceous material, synthesized by the controlled oxidation of graphite [1–6]. It is a non-stoichiometric compound, in which the lamellar structure of graphite is preserved, but its polyaromatic character is lost, as related to the presence of oxygen-containing functional groups [1–8]. The carbon atoms in GO are arranged in a regular, periodic manner. There are strong covalent bonds within the hexagonal layers and weaker interlayer contacts, hydrogen bonds, between intercalated water molecules [9]. Several models have been suggested for the structure of GO, in which oxygen atoms are bonded to the hexagonal layers of carbon atoms as epoxy linkages [2, 5, 8, 10, 11]. According to recent studies, GO consists of intact graphitic regions interspersed with sp^3 hybridized carbons containing hydroxyl and epoxy groups and sp^2 hybridized carbons with carboxyl and carbonyl goups at the sheet edges [12–14]. GO is a hydrophilic material, which may be dispersed in water to form stable colloidal suspensions via exfoliation [2, 10–12, 15]. Similarly to clay minerals, GO readily undergoes intracrystalline swelling and disaggregation and is therefore suitable for the preparation of thin films and polymer nanocomposites [7, 10, 16]. As related to its pronounced cation exchange capacity and intercalation ability, GO has been employed as a host material for the accomodation of long chain aliphatic hydrocarbons and polymers [13, 17, 18]. As related to its favourable properties, GO may also be regarded as a catalyst support material and a promising host for the intercalation of catalytically active transition and noble metal nanoparticles.

The present study is concerned with the immobilization of monodispersed Pd nanoparticles in GO, to be tested as a catalyst in liquid-phase hydrogenation. The synthesis procedure is based on the generation of Pd particles in a micellar system, by applying the cationic surfactant tetradecyltrimethylammonium bromide (C_{14}TABr) as a stabilizer [19, 20].

2 Experimental

GO was prepared from natural graphite flakes (Kropfmühl AG, Germany) according to Brodie's method [1]. For the generation of Pd nanoparticles in GO, an aqueous solution of the precursor K_2PdCl_4 was first added to a C_{14}TABr solution under vigorous stirring, upon which a stable

Á. Mastalir (✉)
Department of Organic Chemistry, University of Szeged, Dóm tér 8, 6720 Szeged, Hungary
e-mail: mastalir@chem.u-szeged.hu

Z. Király · M. Benkő · I. Dékány
Department of Colloid Chemistry, University of Szeged, Aradi vt. 1, 6720 Szeged, Hungary

colloidal system was formed through solubilization. On addition of an excess of $NaBH_4$, reduction of K_2PdCl_4 took place, which resulted in the formation of a stable Pd sol. Stirring was maintained at room temperature for 2 h and then the surfactant-stabilized Pd sol was added dropwise to a dilute aqueous suspension of GO at pH = 10. On addition of the Pd sol to GO, cation exchange took place, which resulted in the formation of a hydrophobic GO organocomplex. Meanwhile, the reduced Pd particles were immobilized in the GO layers. The excess surfactant was removed in ethanol by several centrifugation/redispersion cycles. The above procedure gave rise to the formation of an organophilic Pd–GO sample.

The Pd content of Pd–GO was determined by inductively coupled plasma atomic emission spectroscopy (ICP-AES), with a Jobin Yvon 24 sequential ICP-AES spectrometer at 229.7 nm and 324.3 nm. The Pd content, obtained from the emission intensity by means of a calibration curve, proved to be 0.19%.

X-ray diffraction measurements were performed with a Philips PW 1820 diffractometer at 40 kV and 35 mA (CuK_α radiation, $\lambda = 0.154$ nm). Data were collected in the range $1° < 2\Theta < 30°$ at an interval of 0.01 2Θ. The interplanar spacing d_L was calculated from the first order Bragg reflection by using a PW 1877 automated powder diffraction software.

TEM images were recorded with a Philips CM10 transmission electron microscope (LaB_6 cathode, 100 kV) equipped with a Megaview II digital camera. The sample was dispersed in ethanol and mounted on a Formvar-coated copper grid. The size distribution and the mean particle diameter ($d = \Sigma n_i d_i / \Sigma ni$) were determined for at least 250 particles, by using AnalySIS 3.1. software.

The catalytic performance of Pd–GO was tested in the liquid-phase hydrogenations of 3-hexyne, 4-octyne and 1-phenyl-1-pentyne (all Aldrich products of 99% purity), in an automated vibration reactor [21] at 298 K and 10^5 Pa. The mass of catalyst was 5 mg and the reactant:Pd ratio (S:Pd) was varied between 2,500 and 10,000. The sample was pretreated in 10^5 Pa of static H_2 for 60 min, followed by evacuation. After reintroduction of H_2, 1 cm^3 of toluene was added as a dispersion medium and pretreatment was completed under stirring for 45 min. The reactions were conducted under efficient stirring (1,400 rpm) in order to eliminate mass transport limitations. The H_2 consumption was monitored at a data collection frequency of 0.5 s^{-1}. The initial rates R were determined from the slopes of the H_2 consumptions plotted as a function of reaction time and the turnover frequencies (TOF) were calculated. The product mixture were analyzed by a HP 5890 gas chromatograph equipped with a DB-1 capillary column and a flame ionization detector (FID). The catalytic runs were repeated up to 3 times, the results exhibited a standard deviation of ±3.5%.

3 Results and Discussion

The formation of the organophilic Pd–GO sample is depicted in Fig. 1. Initially, the Pd particles were surrounded with a protective layer of cationic surfactant molecules. Upon mixing the Pd sol with an aqueous GO suspension at pH = 10, the surfactant molecules were released from the metal surface and irreversibly bound to the cation exchanger positions (hydroxyl groups of phenols and carboxyl groups [7]) of GO. Simultaneously, the bare Pd particles were immobilized on the surface of the GO lamellae via adhesion.

It follows that the amount of surfactant cations on the surface sites of GO is equal to its cation exchange capacity. The organic cations render the GO surface organophilic, which facilitates the redispersion of Pd–GO in organic solvents, e.g. toluene. This kind of surface modification makes GO a favourable support material, to be applied in organic catalysis. It may also be noted that the Pd particles were not leached upon applications.

The XRD patterns of GO and Pd–GO are displayed in Fig. 2. For the GO host, a sharp, well defined peak was obtained at $2\Theta = 12.9°$, which corresponds to an interplanar distance (d_L) of 0.69 nm. The absence of the characteristic d_{002} reflection of graphite at 26.6° confirmed that complete oxidation took place [22], resulting in the

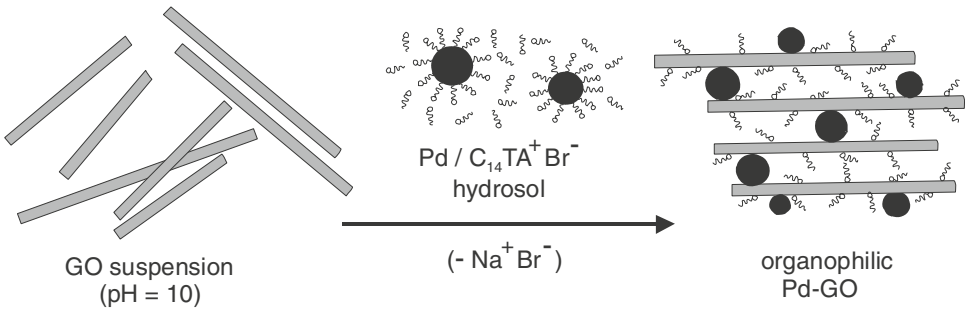

Fig. 1 Proposed mechanism for the formation of organophilic Pd–GO from a GO suspension and a Pd hydrosol, stabilized by the cationic surfactant $C_{14}TABr$

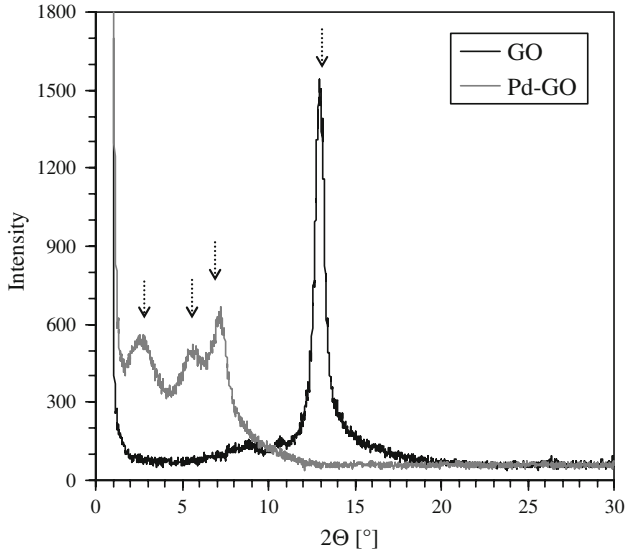

Fig. 2 XRD patterns of GO and Pd–GO

formation of a well-ordered, lamellar structure, which is more open than that of graphite ($d_L = 0.336$ nm) and thus more susceptible to intercalation [22]. For the hydrophobic Pd–GO, three diffraction peaks can be observed at 2.64°, 5.40° and 7.2°.

The first diffraction angle corresponds to $d_L = 3.34$ nm, which can be related to Pd particles situated in the interlamellar space of the GO-organocomplex. Accordingly, the XRD data suggest a mean diameter of 2.65 nm for the intercalated Pd particles, which is in good agreement with that obtained from TEM measurements. The third and the second diffraction angles correspond to the basal spacings 1.23 and 1.63 nm, respectively. These values can be ascribed to the formation of surfactant-GO intercalation compounds, in which the surfactant molecules are situated parallel to the surface of GO to form a flat monolayer and a bilayer, respectively [23]. Alternatively, the occurrence of the second diffraction peak at $2\Theta = 5.40°$ may be regarded as the second order reflection of the first, more intense peak at $2\Theta = 2.64°$. In order to elucidate the occurrence of the second reflection at $2\Theta = 5.40°$, further investigations may be required.

The TEM images of the Pd sol and Pd–GO are shown in Fig. 3.

It may be readily observed for the Pd sol that quasi-spherical, monodispersed nanoparticles were formed. This indicated an efficient size control, exerted by the C_{14}TABr surfactant stabilizer. When the Pd particles were deposited on GO, no aggregation was detected, as the particles fell in the same size range (1–4 nm). Nevertheless, the relative frequencies varied to some extent (Fig.4). For the immobilized Pd particles, the number of 1–1.5 nm particles decreased, whereas the number of 2.5–3 nm particles increased. The mean crystallite diameter for Pd–GO was 2.45 nm, which proved to be only slightly higher than that obtained for the Pd sol (2.18 nm). Accordingly, the dispersion of the Pd–GO sample, calculated as $D = 0.885/d$ [24], was 0.36.

The results of structural characterization indicated that Pd particles were immobilized both on the external surface and in the interlamellar space of GO. As related to the hydrophobic character of Pd–GO, it can be readily dispersed in organic solvents and thus may be utilized as a catalyst in liquid-phase reactions. Alkyne hydrogenations over supported Pd catalysts are typically zero order reactions, for which the initial rate is maintained until complete conversion is achieved [25].

In the present study, the H_2 consumption was monitored as a function of the reaction time. As shown in Fig. 5, linear trends were obtained, indicating that the active centres of Pd–GO were readily accessible for the reactant molecules. However, the initial rates considerably varied with the reactant size [26]. The data obtained for the reactants 3-hexyne, 4-octyne and 1-phenyl-1-pentyne are listed in Table 1.

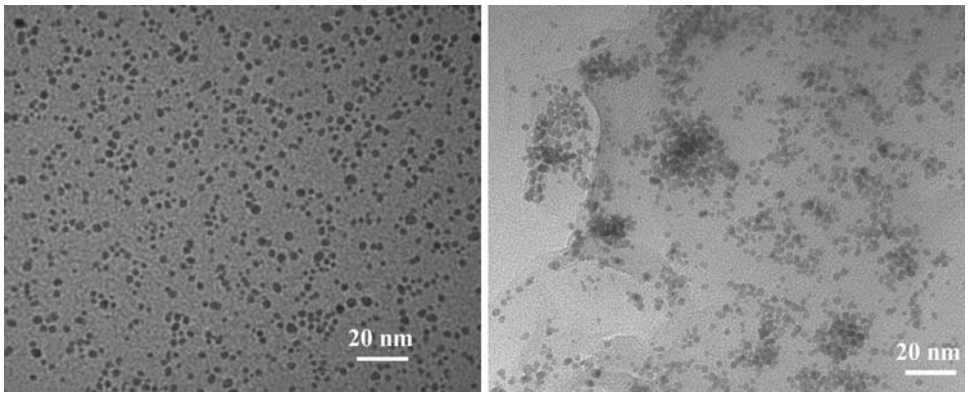

Fig. 3 TEM images of the Pd sol (left) and Pd–GO (right)

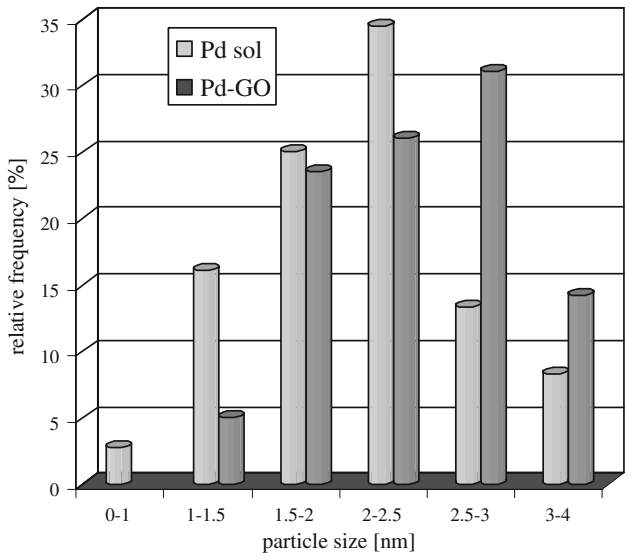

Fig. 4 Particle size distributions of the Pd sol and Pd–GO

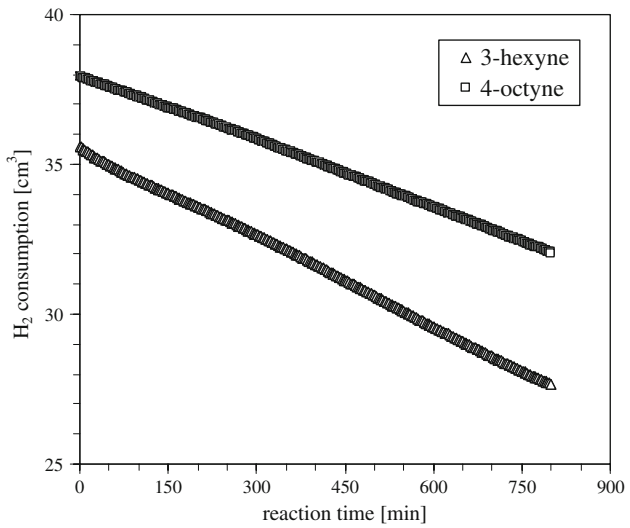

Fig. 5 Hydrogenations of 3-hexyne and 4-octyne over Pd–GO. $m = 5 \times 10^{-3}$ g, S:Pd = 5,000, $p = 10^5$ Pa, $T = 298$ K, solvent: 1 cm^3 of toluene

The conversion for each reactant was found to be strongly dependent on the S:Pd ratio. For the transformations of 3-hexyne and 4-octyne, complete conversions were achieved at S:Pd = 5,000 in 20 and 40 min, respectively. The highest turnover frequencies were determined for the hydrogenation of 3-hexyne. The catalytic activity decreased in the order 3-hexyne > 4-octyne > 1-phenyl-1-pentyne, which corresponds to an increase in the reactant size. This finding can be attributed to the occurrence of interlamellar Pd nanoparticles in Pd–GO, which participate in the reactions as active sites. The major product of alkyne hydrogenation was the *cis*-alkene stereoisomer, for which high stereoselectivities were obtained. An increase in the S:Pd ratio was found to lower the reaction rate and enhance the *cis*-alkene stereoselectivity. The latter values were of a similar order for the reactions of 3-hexyne and 4-octyne, whereas they proved to be somewhat lower for the transformation of 1-phenyl-1-pentyne. This finding may be assigned to steric restrictions, which are likely to affect product desorption and hence, for the aromatic alkyne, diffusion limitations may occur. It may therefore be suggested that Pd–GO is a shape selective catalyst. For the hydrogenations of the above reactants, the catalytic performance of Pd–GO proved to be superior to those of conventional supported Pd catalysts and also to Pd-montmorillonite samples, prepared in a micellar system [26]. The pronounced catalytic activity and the enhanced *cis*-alkene stereoselectivity of Pd–GO may be attributed in part to the effect of the GO host and also to the low Pd loading and the uniform size distribution of the Pd nanoparticles.

4 Conclusions

Monodispersed Pd nanoparticles of 1–4 nm were immobilized in graphite oxide, a layer-structured host material. An efficient particle size control was achieved by using a cationic surfactant stabilizer. The resulting low-loaded, organophilic Pd–GO sample proved to be a highly active and selective catalyst for the liquid-phase hydrogenations of 3-hexyne and 4-octyne. It was ascertained that both interlamellar and external Pd nanoparticles participated in the reactions as active sites. The catalytic activity and the *cis*-alkene stereoselectivity were found to depend on the reactant size, which indicated that Pd–GO was a shape selective catalyst.

Table 1 Hydrogenations of internal alkynes over Pd–GO

Reactant	S:Pd	Time (min)	R (cm^3H_2 $min^{-1}gPd^{-1}$)	TOF (s^{-1})	Conversion (%)	$S_{Cis\text{-}alkene}$ (%)
3-Hexyne	5,000	20	189,017	38	100	94.9
3-Hexyne	10,000	20	78,137	15.7	54.7	98.3
4-Octyne	5,000	40	31,543	6.3	100	93.1
4-Octyne	10,000	40	26,983	5.4	43.8	96.2
1-Phenyl-1-pentyne	2,500	35	8,057	1.6	64.8	82.5
1-Phenyl-1-pentyne	5,000	60	4,148	0.8	44.6	91.3

Acknowledgment This work was supported by the Hungarian Research Fund (OTKA Grants T 047390 and T 068152) and the Bolyai János Foundation.

References

1. Brodie BC (1860) Ann Chim Phys 59:466
2. Hofmann U, Frenzel A (1930) Ber Deut Chem Ges 63:1248
3. Clauss A, Plass R, Boehm HP, Hofmann U, Anorg Z (1957) Allgem Chem 291:205
4. Hummers WS Jr, Offeman RE (1958) J Am Chem Soc 80:1339
5. Boehm HP, Hofmann U (1962) Z Naturforscher B17:150
6. He H, Riedl T, Lerf A, Klinowski J (1996) J Phys Chem 100:19954
7. Szabó T, Tombácz E, Illés E, Dékány I (2006) Carbon 44:537
8. Boehm HP, Clauss A, Fischer G, Hofmann U (1962) In: Proceedings of the Fifth Conference on Carbon. Pergamon Press, Oxford
9. Liu Z, Wang Z-M, Yang X, Ooi K (2002) Langmuir 18:4926
10. Dékány I, Krüger-Grasser R, Weiss A (1998) Colloid Polym Sci 276:570
11. Beckett RJ, Croft RC (1952) J Phys Chem 56:929
12. Stankovich S, Piner RD, Nguyen ST, Ruoff RS (2006) Carbon 44:3342
13. Bourlinos AB, Gournis D, Petridis G, Szabó T, Szeri A, Dékány I (2003) Langmuir 19:6050
14. Lerf A, He H, Forster M, Klinowski J (1998) J Phys Chem B 102:4477
15. Lerf A, Buchsteiner A, Pieper J, Schöttl S, Dékány I, Szabó T, Boehm HP (2006) J Phys Chem Solids 67:1106
16. Kotov NA (2006) Nature 442:254
17. MatsuoY, Hatase K, Sugie Y. Chem Commun (1999) 43
18. Kyotani T, Moriyama H, Tomita A (1997) Carbon 35:1185
19. Király Z, Veisz B, Mastalir Á, Rázga Z, Dékány I (1999) Chem Commun 1925
20. Mastalir Á, Király Z, Szöllősi G, Bartók M (2000) J Catal 194:146
21. Mastalir Á, Király Z (2003) J Catal 220:372
22. Hontoria-Lucas C, López-Peinado AJ, de López-González J, Rojas-Cervantes ML, Martín-Aranda RM (1995) Carbon 33:1585
23. Matsuo Y, Niwa T, Sugie Y (1999) Carbon 37:897
24. Aben PC (1968) J Catal 10:224
25. Carturan G, Facchin G, Cocco GS, Enzo S, Navazio G (1982) J Catal 76:405
26. Mastalir Á, Király Z, Berger F (2004) Appl Catal A: Gen 269:161